An Accurate Propagator for Heterogeneous Media in Full Wavefield Migration

Li, Anyu; Verschuur, Dirk J.; Liu, Xuewei; Abolhassani, Siamak

DOI
10.1109/TGRS.2024.3397887

Publication date
2024

Document Version
Final published version

Published in
IEEE Transactions on Geoscience and Remote Sensing

An Accurate Propagator for Heterogeneous Media in Full Wavefield Migration

Anyu Li, Dirk J. Verschuur, Xuewei Liu, and Siamak Abolhassani

***Abstract*— Since seismic imaging creates an image of the subsurface structure based on information received from the measured wavefield, it is essential to fully utilize the reflected waves. Full Wavefield Modeling (FWMod) was developed with recursive and iterative up-and-down wavefield propagation, using one-way wave propagation, to model both primary and multiple reflections. Using FWMod as the modeling engine, Full Wavefield Migration (FWM) has been introduced to directly image data including internal multiples, where internal multiple crosstalk is suppressed automatically via an inversion-based data-fitting process. This avoids the need for applying internal multiple removal, which is often challenging. Conventional one-way wave propagators calculated in the wavenumber domain, like the phase shift (PS) operator, have limitations when applied to strongly inhomogeneous media. Even when computing a new operator at each lateral grid point, they still suffer difficulties because the medium is assumed to be locally homogeneous. In the past, matrix eigendecomposition has been proposed as a way to create accurate, local velocity-based one-way propagation operators. In this article, an accurate propagator based on eigendecomposition is incorporated into FWMod and FWM. In the numerical examples, four models with strong lateral velocity variations were used to test the propagator. With a comparison of the conventional FWM based on the PS operator with input data including FWMod and a finite-difference (FD) approach, the numerical examples demonstrated that the proposed method has the potential to significantly enhance image reflectivity, suppress internal multiples, and maintain convergence speed during the least-squares inversion.**

***Index Terms*— Eigen-decomposition (ED), full wavefield migration (FWM), propagator, wave equation.**

I. Introduction

CONVENTIONAL seismic migration methods rely on having primary reflection data. To make the data suitable for primary wavefield migration (PWM), extensive research has been carried out to address the issue of multiple reflections (also known as multiples) in both academic and industrial domains. These works remove multiples from the data in a preprocessing stage. Various studies have focused on mitigating surface multiples [1], [2], [3], as well as internal multiples [3], [4]. Surface multiples tend to be stronger as they arise from energy reflecting off the surface, whereas internal multiples are generated between prominent subsurface reflectors. Eliminating internal multiples is more challenging due to limited knowledge of the underlying geometric structures that generate these multiples. However, it is essential to recognize the valuable information embedded in the multiples and leverage it instead of discarding it during imaging.

Verschuur and Berkhout [5] proposed the utilization of surface multiples for imaging purposes. Building upon this idea, Brown and Guitton [6] achieved multiple wavefield migration by employing the least-squares method. In subsequent work, Verschuur and Berkhout [7] presented a novel approach that treats surface multiples as responses to the total upgoing wavefield reflected beneath the surface. This method incorporates mixed input data, encompassing both primary reflections and surface multiples. Lu et al. [8] formulated the imaging of multiples in terms of separated wavefield recordings at the surface and demonstrated it on 3-D field data. Unlike conventional approaches, where multiples are excluded from Green's function, in this method, multiples are regarded as part of the incident wavefield. Consequently, this approach offers improved dual-illumination characteristics. To mitigate interference in the resulting images, a closed-loop approach based on parameter-driven forward modeling of the estimated parameters is employed. Building upon these advancements, Zhang and Schuster [9] and Tu and Herrmann [10] have also embraced similar methodologies to facilitate the mapping of primary wavefields and surface multiples into the subsurface image. It is important to note that this process, inclusive of surface multiples, can still be categorized as model-driven.

Taking internal multiples into account in migration, distortions caused by internal multiples in the subsalt region can be reduced, and additional illumination from internal multiples can be obtained. Berkhout [11] explained how to extend PWM to full wavefield migration (FWM) by considering scattering at each subsurface reflection point in two directions: upward and downward, where the downward reflection generates internal multiples. Based on this concept, Berkhout [12], [13] proposed a series of methods for full wavefield modeling (FWMod) and FWM. In these closed-loop approaches, both surface and internal multiples can be created with the seismic image itself to generate scattering, by using one-way

Manuscript received 15 August 2023; revised 13 December 2023 and 13 March 2024; accepted 4 May 2024. Date of publication 6 May 2024; date of current version 17 May 2024. This work was supported in part by Delphi Consortium from Delft University of Technology, The Netherlands; and in part by China Scholarship Council. *(Corresponding author: Anyu Li.)*

Anyu Li is with the School of Geophysics and Information Technology, China University of Geosciences, Beijing 100083, China, and also with the Department of Imaging Physics, Delft University of Technology, 2628 CN Delft, The Netherlands (e-mail: li_anyu@foxmail.com).

Dirk J. Verschuur and Siamak Abolhassani are with the Department of Imaging Physics, Delft University of Technology, 2628 CN Delft, The Netherlands.

Xuewei Liu is with the School of Geophysics and Information Technology, China University of Geosciences, Beijing 100083, China.

Digital Object Identifier 10.1109/TGRS.2024.3397887

wavefield propagators instead of relying on finite-difference (FD) modeling. Through iteration, arbitrary-order multiples can be simulated and reflectivity can be estimated such that all reflection events (primary reflections and multiples) conform to the observed data. In contrast to data-driven multiple removal methods, FWM is not limited by densely sampled sources and can handle complete wavefields with both surface and internal multiples, assuming nonlinearity in reflectivity. Davydenko and Verschuur [14] further developed this concept and included angle-dependent imaging in FWM. Davydenko and Verschuur [15] verified the application potential of FWM by a field data example including internal multiples.

The propagator plays a crucial role in FWM because both the primaries and multiples are generated and extrapolated by repeatedly utilizing it. However, the conventional one-way wave operators used in FWM, such as phase shift (PS) migration or PS plus interpolation migration, have limitations when dealing with strongly inhomogeneous media due to the assumption of a local homogeneous velocity at each grid point, as they perform an inverse spatial Fourier transform on operators modeled in the wavenumber domain [16], [17]. The classical one-way wave propagators and their optimized methods involved in wave-equation migration were generally based on the wavefield extrapolation formula for calculating the wavefield with a higher-order mathematical series [18], [19], [20], [21], [22]. These methods commonly use a reference velocity to replace the accurate velocity in the horizontal direction, leading to errors in inhomogeneous media.

To overcome this issue, the common solution is to calculate a new operator on all grid points. However, when encountering strong lateral inhomogeneities, the structure of the PS propagator matrix departs from being Toeplitz and instead, each row comprises a different local convolutional operator. The length of this operator influences the accuracy with which lateral inhomogeneities can be addressed; shorter operators are better suited for handling such variations but using short operators can introduce numerical errors during propagation, especially at large angles [23].

To mitigate this, a local velocity-based one-way wave propagator has been proposed, which calculates an accurate solution at each grid node via eigen decomposition of the propagator matrix, and can accommodate arbitrarily lateral velocity variations [24], [25], [26]. In this study, we integrate such one-way wave eigen-decomposition (ED) operators into the FWMod and FWM frameworks to make them better suited for heterogeneous media, resulting in improved imaging amplitude and recovery of reflectivity while still maintaining the ability to suppress internal multiples.

II. Method

A. Full Wavefield Modeling

Conventional wavefield modeling inside a least-squares migration algorithm is based on the Born approximation, where an incident wavefield is multiplied by the reflectivity at each grid point before being extrapolated forward to the surface. These diffraction responses will produce the simulated primaries upon superposition. This process is also known as "de-migration" because it enables the data to be reconstructed based on the reflectivity approximated during the imaging procedure. The simulated and measured data are compared, and the residual data is reimaged to update the reflectivity for the subsequent iteration. This method also permits the management of surface multiples by merely modifying the source-side wavefield [7], [8], however, it does not include internal multiples.

FWMod extends such an approach by including also internal multiples in the modeling process. It involves decomposing the wavefield into two components, namely a downgoing component represented by P^+ and an upgoing component represented by P^-. This representation is made regarding a preferred direction, which is typically the vertical direction. The source extrapolation equation can be expressed for a given shot gathered at one frequency component [12]

$$P^{\pm}(z_m, z_0) = \mathbf{W}^{\pm}(z_m, z_0) S^{\pm}(z) + \sum_{n=0}^{m-1} \mathbf{W}^{\pm}(z_m, z_n) \delta S^{\pm}(z_m, z_0) \tag{1}$$

where the equation involves a (possible) physically induced source at depth level z, denoted by S. In addition, there is a secondary source, δS, triggered by the medium in response to an incident wavefield. The $+$ indicates downgoing waves, and the $-$ represents the upgoing ones. The matrices $\mathbf{W}^{\pm}(\mathbf{z}_\mathbf{m}^{\mp}, \mathbf{z_0})$ represent the scattering-free downward and upward propagation operators, respectively, between depth levels z_0 and $z_m (n > m)$. The secondary source is connected to the medium parameters through the following relationship:

$$\delta S^{\pm}(z_n, z_0) = \mathbf{R}^{\cap/\cup}(z_n, z_n) P^{\mp}(z_n; z_0) + \delta \mathbf{T}^{\pm}(z_n, z_n) P^{\pm}(z_n; z) \tag{2}$$

where $\mathbf{R}$ and $\mathbf{T}$ represent the vertical components of reflection and transmission operators and the differential transmission operator $\delta\mathbf{T}$ is defined as $\mathbf{T} = \mathbf{I} + \delta\mathbf{T}$.

Furthermore, for small offsets or under the acoustic approximation, we can replace $\mathbf{T}^+$ and $\mathbf{T}^-$ with the upgoing reflection operators $\mathbf{R}^{\cup}$ and downgoing version $\mathbf{R}^{\cap}$, respectively,

$$\begin{cases} \mathbf{T}^+ = \mathbf{I} + \mathbf{R}^{\cup} \\ \mathbf{T}^- = \mathbf{I} + \mathbf{R}^{\cap} \\ \delta\mathbf{T}^+ = \mathbf{R}^{\cup} \\ \delta\mathbf{T}^- = \mathbf{R}^{\cap} = -\mathbf{R}^{\cup} \end{cases} \tag{3}$$

and then (2) can be simplified as

$$\delta S(z_n, z_0) = \mathbf{R}^{\cup}(z_n, z_n) P^+(z_n; z_0) + \mathbf{R}^{\cap}(z_n, z_n) P^-(z_n; z). \tag{4}$$

Also as shown in Fig. 1, every subsurface grid point considers the complete wavefield connection. Any depth level z_n may be illuminated from above by downgoing wavefield P^+ and from below by upgoing wavefield P^-, originating from the same physical experiment. The total wavefields and potential scattering exit this depth level in both directions.

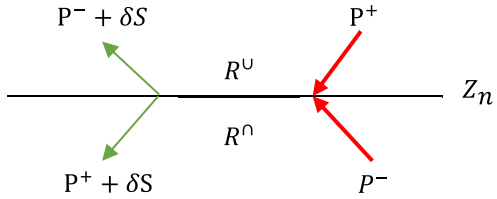

Fig. 1. Wavefields and operators in FWMod related to one depth level.

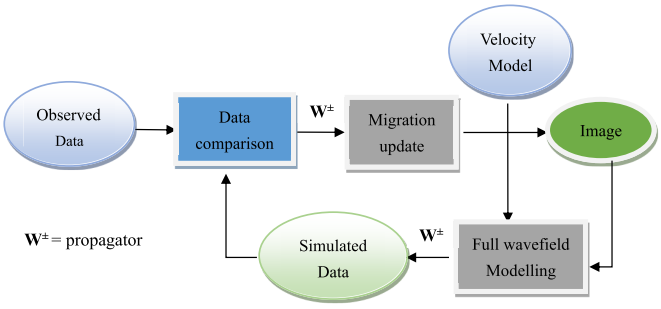

Fig. 2. FWM flowchart.

B. Full Wavefield Migration

FWM is a closed-loop method for a standard inversion-based imaging technique based on least-squares migration, for which the flowchart is given in Fig. 2.

In this imaging process, the complete wavefield propagation is taken into account at each subsurface grid point. Not only primary waves but also internal multiple waves are considered, resulting in a more complete illumination and a more complete description of the measured data. In the closed-loop flow of the full-wavefield migration algorithm in Fig. 2, with the external input data, the gradient and least-squares objective function is obtained by using the difference of the input "measured" data and the full-wavefield forward modeling result, and from this residual—via backpropagation into the subsurface—the reflectivity is updated see more details in [13] and [14]. Thus, FWM works by minimizing the difference between the observed data and the forward data.

The objective function can be described as

$$J = \sum_{\omega} \sum_{k} \Delta P_k \Delta P_k^H \tag{5}$$

where H stands for conjugate transpose, and ΔP is the difference between the observed data and modeled data (i.e., the data residual) for shot number k

$$\Delta P_k = P_{k\text{obs}} - P_{k\text{mod}}. \tag{6}$$

C. From PS to ED Propagator

Computing wavefields in neighboring layers involves using a one-way wave propagator in FWM, which can be written as [27]

$$\mathbf{W}^{\pm} = e^{\mp i \mathbf{\Lambda} \Delta z} \tag{7}$$

where Δz is the depth step and Λ represents the square root operator, also called vertical wavenumber in the PS migration method.

The conventional PS operator assumes a locally homogeneous medium within a specific region surrounding each lateral position so that a spatial Fourier transform can be applied to calculate in the wavenumber domain. To deal with lateral inhomogeneities, the structure of the propagator matrix changes from Toeplitz to local convolution operators in each row by reducing the length of the PS operator. However, short operators during propagation may result in numerical errors [28].

To avoid such issues, here we use an eigen decomposition (ED) method to directly calculate the one-way wave operator in the space domain [24], [25], [26]. With the relationship of the Helmholtz operator Λ^2, as

$$\mathbf{\Lambda}^2 = \frac{\omega^2}{v(x)^2} + \frac{\partial^2}{\partial x^2} \tag{8}$$

in which a second-order discretization of $\partial^2/\partial x^2$ is included, this can be written for a single depth level as

$$\mathbf{\Lambda}^2 = \begin{bmatrix} \frac{\omega^2}{v^2(x_1)} & 0 & \cdots & 0 \\ 0 & \frac{\omega^2}{v^2(x_2)} & \cdots & 0 \\ \vdots & \vdots & \ddots & \vdots \\ 0 & 0 & \cdots & \frac{\omega^2}{v^2(x_n)} \end{bmatrix} + \begin{bmatrix} \frac{-2}{(\Delta x)^2} & \frac{1}{(\Delta x)^2} & 0 & 0 \\ \frac{1}{(\Delta x)^2} & \frac{-2}{(\Delta x)^2} & \ddots & 0 \\ 0 & \ddots & \ddots & \frac{1}{(\Delta x)^2} \\ 0 & 0 & \frac{1}{(\Delta x)^2} & \frac{-2}{(\Delta x)^2} \end{bmatrix}. \tag{9}$$

This matrix can effectively manage variations in lateral velocity in the horizontal direction, thanks to the diagonal elements contained within the matrix. These diagonal elements correspond to all velocity points located at a specific depth. Note that for clarity the matrix is constructed using a second-order FD discretization technique. Still, to improve the accuracy for FWMod and FWM, it is recommended to substitute this with a higher-order discretization method.

Using linear algebra theory, the self-adjoint matrix $\mathbf{\Lambda}^2$ can be factorized into the product of its eigenvalues and eigenvectors as

$$\mathbf{\Lambda}^2 = \mathbf{V}\mathbf{M}\mathbf{V}^T \tag{10}$$

where the matrix $\mathbf{M}$ and $\mathbf{V}$, respectively, denote the eigenvalues and eigenvectors of $\mathbf{\Lambda}^2$, and the superscript T represents the matrix transpose. Using the matrix decomposition theory framework, the eigenvalues and eigenvectors of the subfunctions can be represented as follows:

$$\mathbf{\Lambda} = \mathbf{V}\sqrt{\mathbf{M}}\mathbf{V}^T \tag{11}$$

$$\mathbf{W}^{\pm} = \mathbf{V} e^{\mp i \sqrt{\mathbf{M}} \Delta z} \mathbf{V}^T. \tag{12}$$

Note that the traditional PS operator needs an extra filter process to address the issue of evanescent waves that lead to

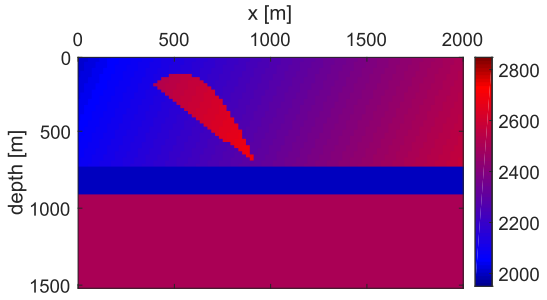

Fig. 3. Velocity model.

instability, as they grow exponentially, such as an $f-k$ filter. However, in ED propagator-based one-way wave migration, the growth of evanescent waves is attributed to complex-valued eigenvalues. Therefore, it is convenient to remove them by keeping the real-valued eigenvalues and disregarding the complex-valued ones.

III. Numerical Examples

In this section, we will discuss the features of the ED-based FWM scheme in four experiments, including an inverse-crime that uses FWMod data as observed data in FWM, and three noninverse-crime processes in which the FD method [29] is utilized to generate observed data served as input for FWM. Each of the examples highlights certain aspects of the proposed methodology.

A. FWM With FWMod (Inverse Crime)

First, we consider the inverse-crime situation, where the input data is modeled with FWMod. The size of the velocity model is 1500 × 2000 m with a grid of 20 × 20 m, which has a strong lateral velocity contrast and steep dipping angles, as shown in Fig. 3. We use this model to verify the imaging performance of the proposed FWM algorithm under ideal circumstances. The shot distance and receiver distance are 100 and 20 m, respectively, and as a source, we use a Ricker wavelet with a peak frequency of 30 Hz. A series of shot-gather records, generated by FWMod with up to fourth-order multiples, is shown in Fig. 4. The primary wavefield, the first- and fourth-order multiples, are shown in Fig. 4(a)–(c), respectively. The multiples only, calculated via the difference between the fourth order of full wavefield and primary wavefield, are displayed in Fig. 4(d).

The true reflectivity model is shown in Fig. 5(a). Fig. 5(b) and (c) shows the imaging results for 1 and 15 iterations of FWM using the ED operator. Note that the internal multiple crosstalks observed in the image after one iteration can be considered the standard depth migration result [Fig. 5(b)] and is properly suppressed during the further iterations of FWM. The difference between the true reflectivity and the estimated reflectivity after using the proposed ED operator in the 1st and 15th iterations is shown in Fig. 6(a) and (b). This proves that our method can correctly recover reflectivity.

Fig. 6(c) illustrates the imaging amplitude at a specific location on the x-axis ($x = 860$ m), while Fig. 6(d) depicts

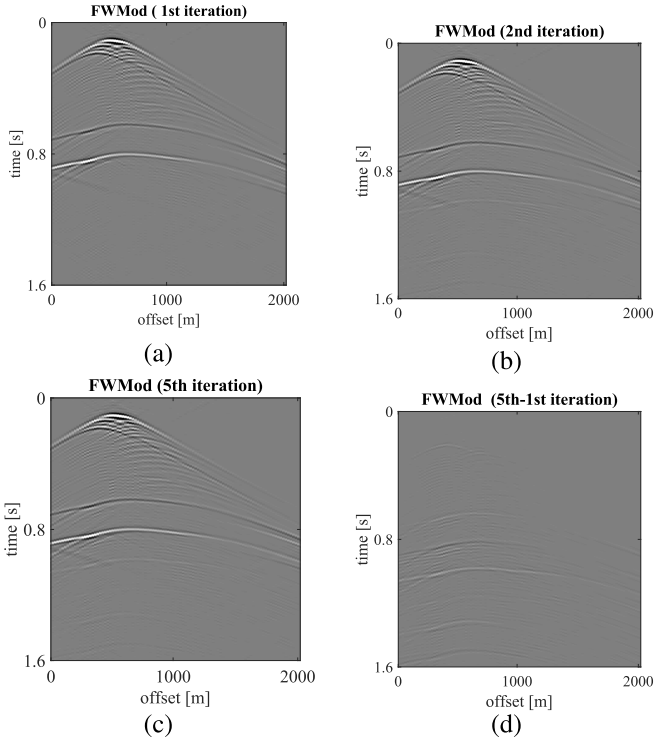

Fig. 4. FWMod using ED propagator. (a) Only primary wavefield, (b) first-order multiple and primary waves, (c) fifth-order multiple and primary waves, and (d) only multiples.

TABLE I
Computational Cost Comparison

	Computing time	Used Memory
PS	38 s	7207 MB
ED	112 s	9088 MB

the reflectivity at a particular depth of 740 m. The proposed algorithm can handle strong velocity contrasts, accurately show the structure, and achieve true reflectivity, as shown by a comparison with the real model and imaging section. The amplitude and reflectivity curves show that the algorithm deals with transmission compensation and internal multiple imaging. This is how we can get a real result for amplitude migration.

The costs of computing and memory are another concern for industry. The computational comparison between the utilized ED and conventional PS operator is shown in Table I. It illustrates that the ED operator is only about three times slower than that of using the PS propagator, with a little more memory occupied, which is acceptable for the industry to improve the image result.

B. Single Impulse Test

In the next example, we show the accuracy of the ED-based propagator at high angles via a migration impulse response. The velocity model presented in Fig. 7 is generated using the function $v(x, z) = 15x + 2z + 1500$, which has a strong lateral velocity variation ranging from 1500 to 4500 m/s. We use a single trace with one wavelet as a receiver wavefield

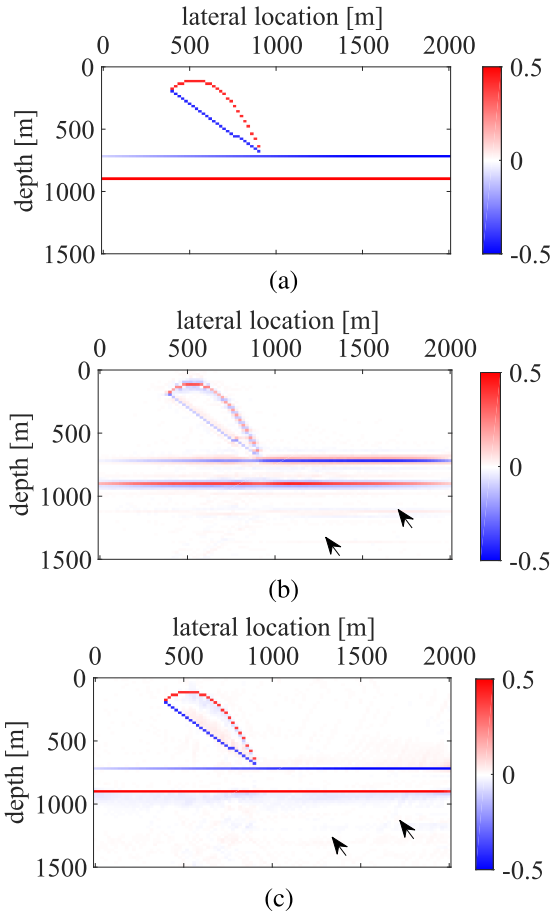

Fig. 5. (a) True reflectivity model, the imaging section after, (b) 1st iteration, and (c) 15th iterations of FWM using the ED propagator.

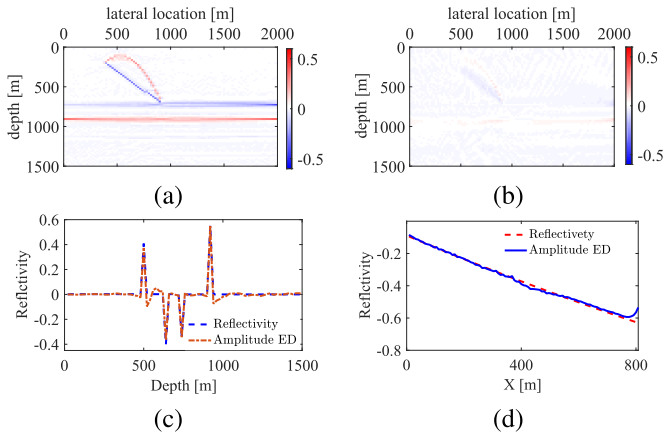

Fig. 6. Difference between the true reflectivity and the estimated reflectivity after (a) 1st and (b) 15th iterations of FWM. Imaging reflectivity comparisons were extracted at (c) $x = 860$ m and (d) depth $= 740$ m after the 15th iteration of FWM, respectively.

with a maximum frequency of 25 Hz to test the suitability of the ED-based propagator.

Fig. 8 exhibits the real and imaginary components of the PS and ED propagators at one depth level with $\Delta z = 10$ m for a frequency of 10 Hz. We observe that the imaginary components of the two operators are very similar, but the real parts are quite different. Considering that the wave propagation

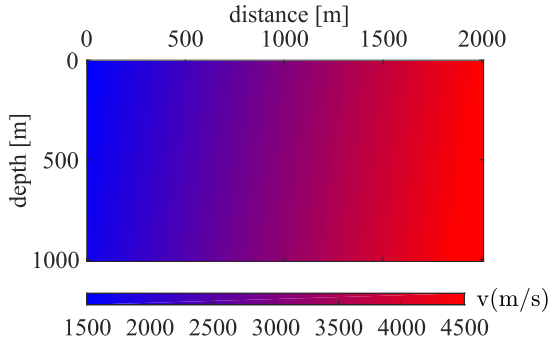

Fig. 7. Inhomogeneous velocity model with strong lateral velocity gradients.

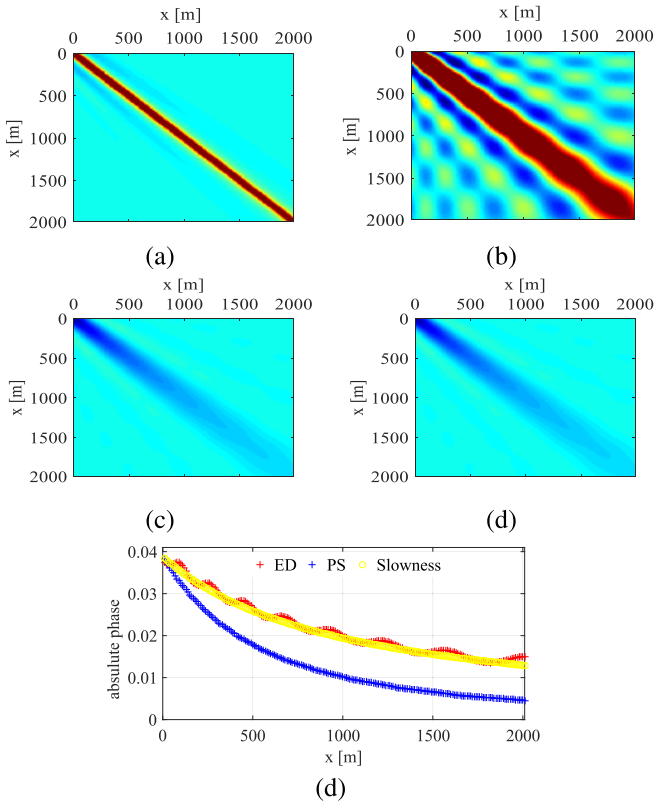

Fig. 8. Propagator comparison at 10 Hz. (a) Real part of PS. (b) Real part of ED. (c) Imaginary part of PS. (d) Imaginary part of ED. (e) Comparison of the absolute phase of ED and PS operators with slowness.

phase depends on both real and imaginary parts of the complex operator, and should be consistent with the medium velocity. Therefore, as shown in Fig. 8(e), the two operators' absolute phases are used to compare with the trends of slowness, in which we can see the perfect consistency between the absolute phase calculated by the utilized ED operator and the slowness variations.

Fig. 9 represents a comparison of the migration impulse response with a single wavelet in the middle of the model, in which the PS, ED, and FD methods are involved. Taking the FD results as a standard, we can see that the ED propagator can achieve a more accurate wavefront than the PS operator, as indicated by the gray arrows at angles close to 90°, where we see that the wavefront from the PS propagator becomes inaccurate and is fading out.

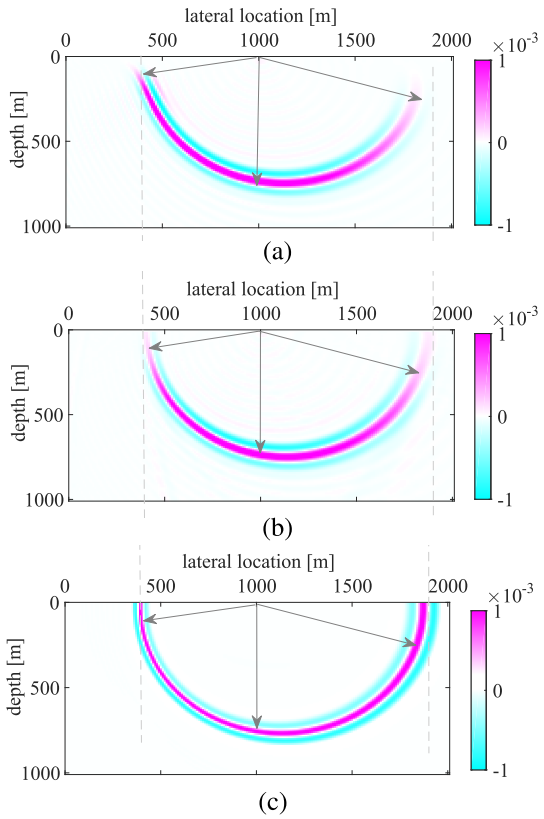

Fig. 9. Migration impulse responses of (a) PS, (b) ED, and (c) FD method.

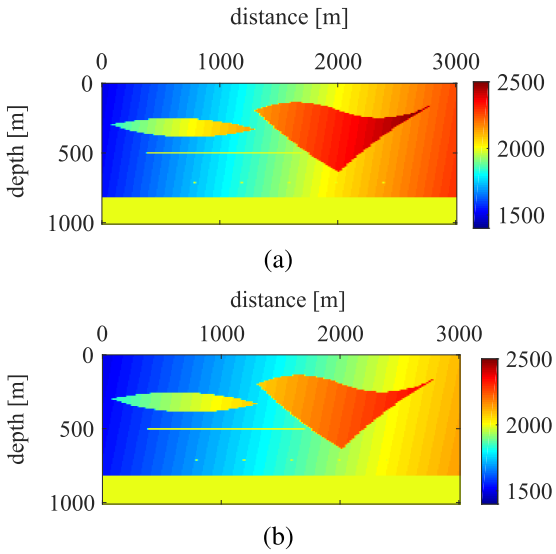

Fig. 10. (a) Accurate and (b) erroneous velocity model.

C. Varying-Velocity Background Model With FD Data

The next velocity model utilized in this study has a size of 1000 × 3000 m with a grid size of 5 × 10 m. The accurate model exhibits steep dipping angles with a laterally varying background velocity contrast, as shown in Fig. 10(a). The erroneous model which changed lateral background velocity shown in Fig. 10(b) is also employed to evaluate the efficacy of the proposed FWM algorithm in terms of imaging performance, under the situation of including a kinematic

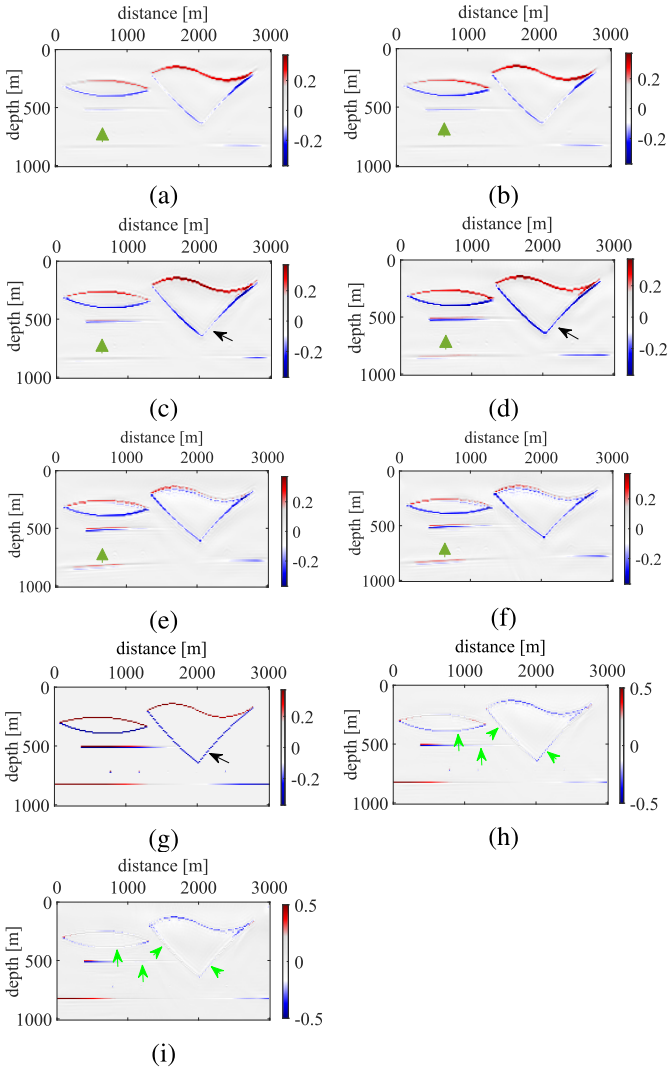

Fig. 11. Imaging results after the first round of iteration of FWM using (a) PS and (b) ED operators based on an accurate velocity model; the imaging section after three rounds of iterations of FWM using (c) PS operator and (d) ED operators based on accurate velocity model; the imaging section after 3 iterations of FWM using (e) PS operator and (f) ED operators based on the erroneous velocity model. (g) True reflectivity model; the difference between the true reflectivity and the estimated reflectivity of (h) PS and (i) ED propagators based on the accurate velocity model.

error. The shot and receiver distances are, respectively, set at 50 and 10 m.

The imaging results can be seen in Fig. 11. Fig. 11(a) and (b) shows comparisons of the imaging sections that were obtained after a single round of FWM using the PS and ED propagators. Fig. 11(c) and (d) are obtained using the PS and the ED propagators after 3 iterations based on the accurate velocity model, respectively. These four pictures reveal that both propagators can properly deal with the internal multiples, as indicated by the deep green signs. However, the ED operator can produce more accurate reflectivity, especially for the dipping reflectors of the subsurface, than the PS operator, as indicated by the black arrows. Fig. 11(e) and (f) are the imaging results of corresponding situations with the erroneous model, in which a kinematic error is inserted. Although it shifts the positioning

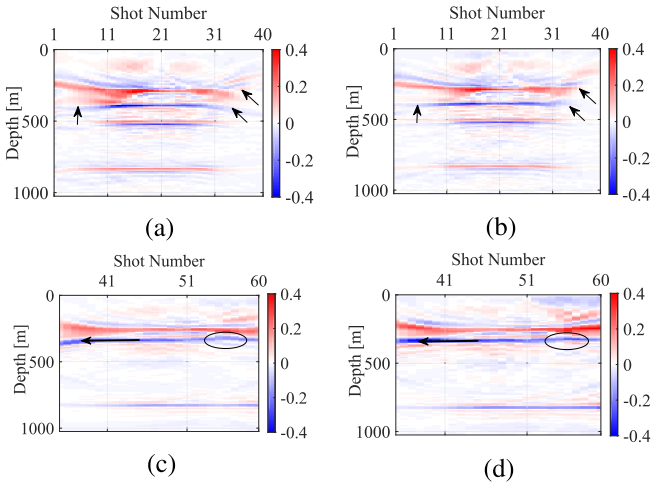

Fig. 12. Shot-domain CIG extracted at $x = 1000$ m from (a) PS and (b) ED operator-based FWM methods; shot-domain CIG extracted at $x = 2500$ m from (c) PS and (d) ED operator-based FWM methods.

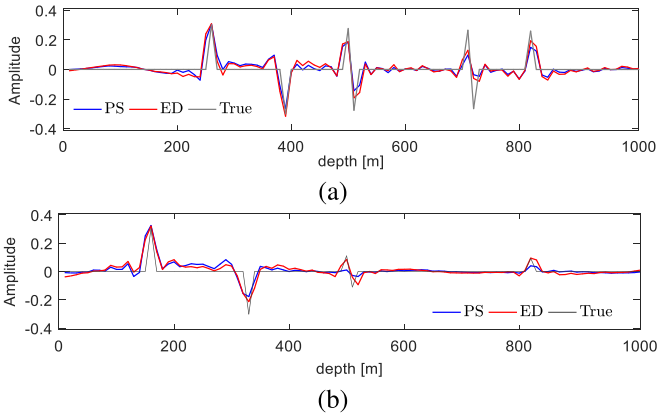

Fig. 13. Difference between true reflectivity and estimated reflectivity after 3 iterations at (a) $x = 800$ m, and (b) $x = 1500$ m.

and damages the image quality of the reflections. Still, from the two subfigures, we can see a slight improvement in image results, and reveal that the ED operator is still superior, even when using an erroneous velocity model. Fig. 11(g) shows the true reflectivity model, which is used to judge how well the imaging methods work. In the meantime, we calculate the difference between the true reflectivity and estimated reflectivity of the PS and ED propagators, as presented in Fig. 11(h) and (i), respectively. From the different parts, the light green arrows show that the ED operator-based FWM algorithm can get a more accurate result than the PS operator.

Additionally, Fig. 12 presents the shot-domain common image gathers (CIGs) to demonstrate the effectiveness of amplitude correctness, enhancing the illustration through the moveout quality of the kinematic behavior of the migration methods. Shot domain CIG represents information extracted at a specific lateral position from different single-shot images, where seismic events should appear flat. Comparing the CIG generated from the two operator-based FWM at positions of $x = 1000$ m and $x = 2500$ m respectively, it is evident that the FWM using the ED operator creates flatter gathers than using the PS operator, as indicated by the black arrows and

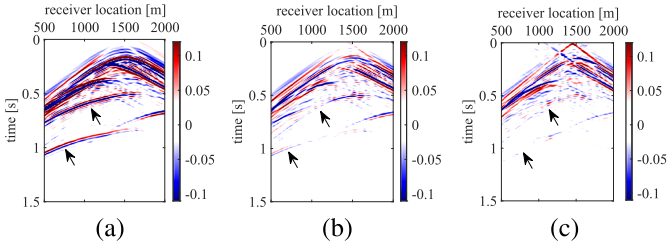

Fig. 14. (a) Observed data and residual data using (b) PS and (c) ED propagators after 3 iterations.

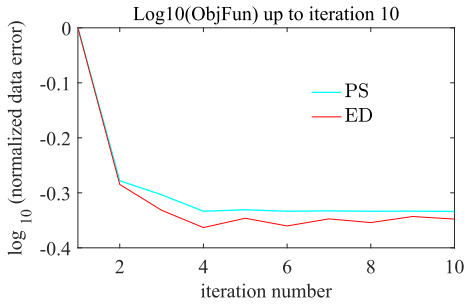

Fig. 15. Objective function when FWM uses the ED operators, compared with the conventional PS operators.

ellipses. This figure confirms the ED operator's superiority in terms of the kinematic behavior and AVA/AVO effect.

Then, Fig. 13(a) and (b) shows comparisons of the true reflectivity and the estimated reflectivity for the two types of propagators after three iterative cycles. The data was taken at $x = 800$ m and $x = 1500$ m. This figure further confirms the better recovery ability of amplitudes by using the ED operator, from the comparison of amplitude curves with true reflectivity.

Moreover, Fig. 14 shows a comparison between observed data and residual data from using both PS and ED propagators in FWM after 3 iterations. In this figure, the residual data of the ED propagator is cleaner than that of the PS operator. That means the wavefield generated by the ED operator is closer to the FD-generated observed data. Fig. 15 presents a comparison of the objective function obtained using the two types of propagators in FWM. The objective function serves as a gauge of the image's quality after the imaging process. A lower objective function value indicates that the imaging result is more accurate and closer to true reflectivity. We can see that the proposed method achieves a lower objective function value compared to the conventional PS operator. It indicates that the proposed method is more effective in describing the input data and, thereby, producing more accurate imaging results.

D. SEG-EAGE Salt Model Using FD Data

The SEG-EAGE salt model (see [30]) comprises a typical velocity gradient overlaid by a tetragonal salt with a significantly higher wave velocity. The selected slice from this 3-D model we used in this study is shown in Fig. 16. In this example, the observed data is generated using the finite-difference method with a grid size of 5 × 5 m. The receiver interval is 20 m, and the shot distance is 100 m, with a sampling rate of 4 ms, using the Ricker wavelet with a peak frequency of 30 Hz.

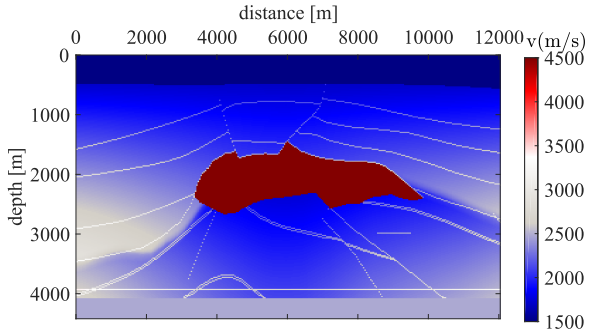

Fig. 16. True velocity model extracted from the SEG-EAGE salt model.

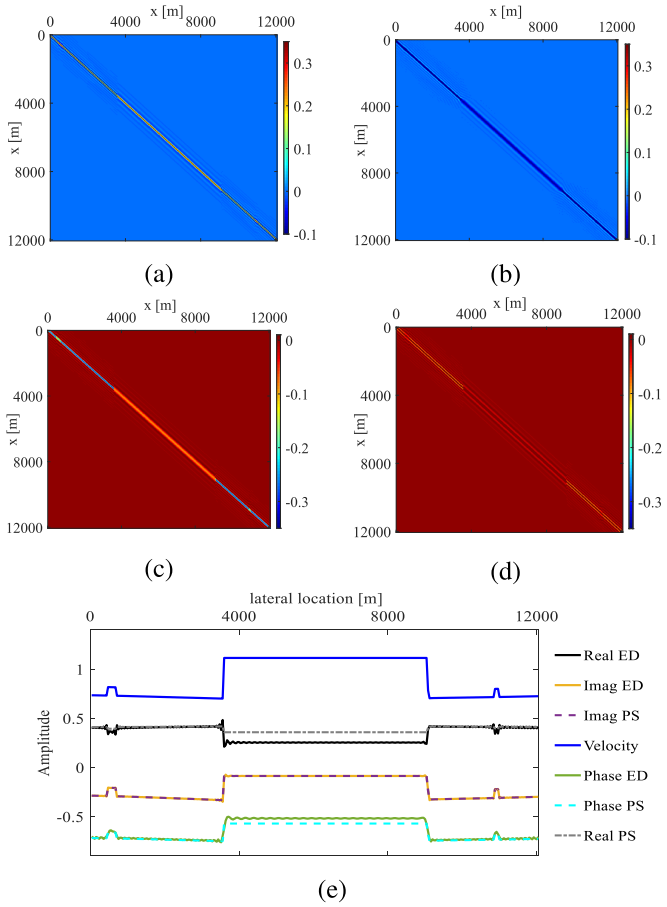

Fig. 17. Representations of the complex-valued propagation operator for the depth slice at $z = 2000$ m and frequency 15 Hz. The real part of (a) PS and (b) ED operators; the imaginary part of (c) PS operator and (d) ED operator. (e) Comparison of the diagonal elements and phases of the real and imaginary components of PS and ED propagators, together with the relative velocity variations (in blue) at this depth slice.

Fig. 17(a) and (b) shows the real components of the complex propagation PS and ED operator at a depth of 2000 m with a frequency of 15 Hz. Similarly, Fig. 17(c) and (d) are the imaginary parts of the two operators. To provide a clearer understanding of the characteristics of the two propagators, we extract the diagonal elements as shown in Fig. 17(e). By looking at the phases of PS and ED propagators along with changes in relative lateral velocity (shown in blue), we can see that both propagators are in line with changes in velocity. Note that the differences between the ED and PS operators are only visible in the real part, while the imaginary parts are virtually identical.

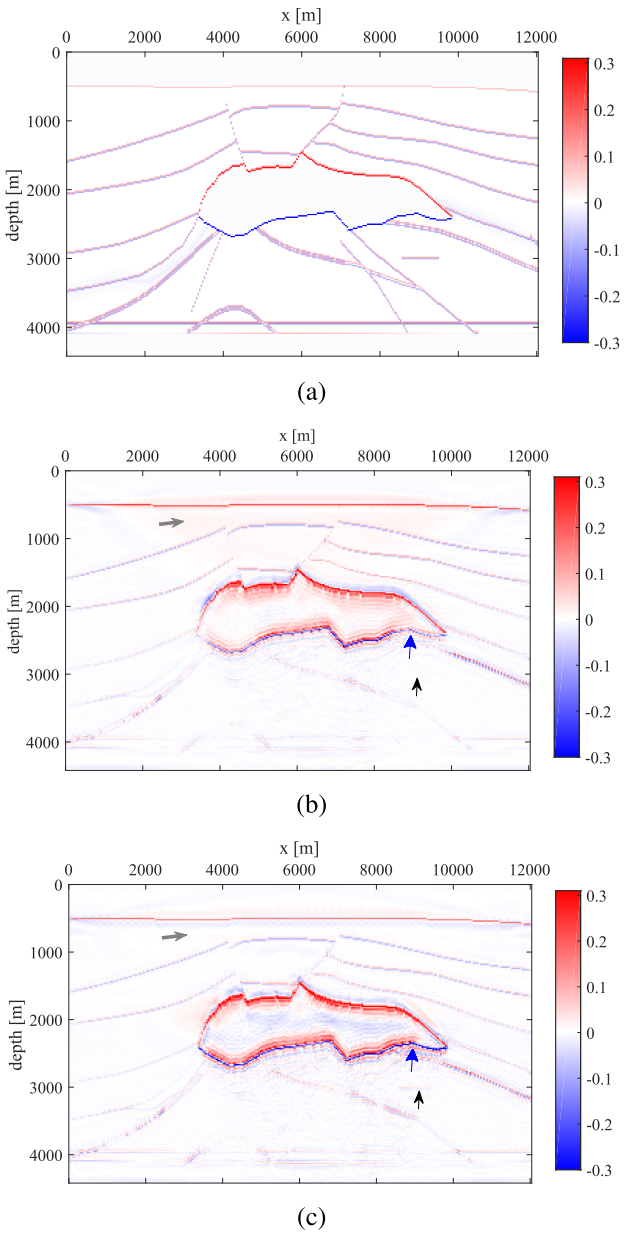

Fig. 18. (a) True reflectivity model and the imaging section after 10 iterations of FWM using (b) PS and (c) ED propagators.

Fig. 18 presents the true reflectivity model, showing the normal incidence reflectivity, along with the imaging sections after 10 iterations of the conventional PS operator and the proposed ED operator. As shown in Fig. 18(b) and (c), the image produced by the ED operators exhibits a more accurate representation of the subsalt structures, as indicated by the black arrows, corresponding to the PS operator. These findings demonstrate the superiority of the proposed ED operator in improving true amplitude imaging capabilities and image fidelity in complex subsurface structures.

IV. Conclusion

This study presents a novel approach for enhancing FWM by incorporating an eigendecomposition-based one-way wave

propagator. The method entails the computation of the eigenvalues and eigenvectors of the Helmholtz operator to construct an operator that accurately characterizes the behavior of the wavefield during subsurface propagation. This technique improves true amplitude imaging capabilities by considering the lateral velocity heterogeneity in the subsurface model, instead of making a locally laterally homogeneous velocity assumption. Numerical tests, like the "inverse crime" process, which used data modeled with the FWMod engine to reveal the method's better performance in FWM, show that the proposed method works well. The incorporated ED operator was also tested using FD-modeled observed data. The implausible response tests worked to verify the proposed algorithm's image angle. The simple model with accurate and erroneous velocity illustrated that the operator worked better for reflectors that were dipping steeply while still maintaining the FWM approach's ability to suppress internal multiple signals. Furthermore, the SEG-EAGE-salt model example illustrated the good performance of our proposed method. Meanwhile, the difference between the obtained ED and PS propagators was analyzed to provide insights into why using the ED operator can produce more accurate results.

ACKNOWLEDGMENT

The authors would like to thank Delphi Research Consortium and China Scholarship Council for supporting this research. They also acknowledge Dr. Joost van der Neut, Leo Hoogerbrugge, Dong Zhang, and Ali Alfaraj for their helpful discussions and contributions.

REFERENCES

[1] J. R. Berryhill and Y. C. Kim, "Deep-water peg legs and multiples: Emulation and suppression," *Geophysics*, vol. 51, no. 12, pp. 2177–2184, Dec. 1986.

[2] D. J. Verschuur, A. J. Berkhout, and C. P. A. Wapenaar, "Adaptive surface-related multiple elimination," *Geophysics*, vol. 57, no. 9, pp. 1166–1177, Sep. 1992.

[3] A. B. Weglein, F. A. Gasparotto, P. M. Carvalho, and R. H. Stolt, "An inverse-scattering series method for attenuating multiples in seismic reflection data," *Geophysics*, vol. 62, no. 6, pp. 1975–1989, Nov. 1997.

[4] D. J. Verschuur and A. J. Berkhout, "Removal of internal multiples with the common-focus-point (CFP) approach: Part 2—Application strategies and data examples," *Geophysics*, vol. 70, no. 3, pp. V61–V72, May 2005.

[5] D. J. Vershuur and A. J. Berkhout, "Multiple technology: Part 1, estimation of multiple reflections," in *Proc. SEG Tech. Program Expanded Abstr.*, Jan. 1994, pp. 1493–1496.

[6] M. P. Brown and A. Guitton, "Least-squares joint imaging of multiples and primaries," *Geophysics*, vol. 70, no. 5, pp. S79–S89, Sep. 2005.

[7] D. J. Verschuur and A. J. Berkhout, "Seismic migration of blended shot records with surface-related multiple scattering," *Geophysics*, vol. 76, no. 1, pp. A7–A13, Jan. 2011.

[8] S. Lu, D. N. Whitmore, A. A. Valenciano, and N. Chemingui, "Separated-wavefield imaging using primary and multiple energy," *Lead. Edge*, vol. 34, no. 7, pp. 770–778, Jul. 2015.

[9] D. Zhang and G. T. Schuster, "Least-squares reverse time migration of multiples," *Geophysics*, vol. 79, no. 1, pp. S11–S21, Jan. 2014.

[10] N. Tu and F. J. Herrmann, "Fast imaging with surface-related multiples by sparse inversion," *Geophys. J. Int.*, vol. 201, no. 1, pp. 304–317, Feb. 2015.

[11] A. J. Berkhout, "Combining full wavefield migration and full waveform inversion, a glance into the future of seismic imaging," *Geophysics*, vol. 77, no. 2, pp. S43–S50, Mar. 2012.

[12] A. Berkhout, "Review paper: An outlook on the future of seismic imaging," *III: Joint Migration Inversion: Geophys. Prospecting*, vol. 62, pp. 950–971, Jan. 2014.

[13] A. J. Berkhout, "Review paper: An outlook on the future of seismic imaging—Part II: Full-wavefield migration," *Geophys. Prospecting*, vol. 62, no. 5, pp. 931–949, Sep. 2014.

[14] M. Davydenko and D. J. Verschuur, "Full-wavefield migration: Using surface and internal multiples in imaging," *Geophys. Prospecting*, vol. 65, no. 1, pp. 7–21, Jan. 2017.

[15] M. Davydenko and D. J. Verschuur, "Including and using internal multiples in closed-loop imaging—Field data examples," *Geophysics*, vol. 83, no. 4, pp. R297–R305, Jul. 2018.

[16] J. Gazdag, "Wave equation migration with the phase-shift method," *Geophysics*, vol. 43, no. 7, pp. 1342–1351, 1978.

[17] J. Gazdag and P. Sguazzero, "Migration of seismic data by phase shift plus interpolation," *Geophysics*, vol. 49, no. 2, pp. 124–131, Feb. 1984.

[18] P. L. Stoffa, J. T. Fokkema, R. M. de Luna Freire, and W. P. Kessinger, "Split-step Fourier migration," *Geophysics*, vol. 55, no. 4, pp. 410–421, Apr. 1990.

[19] D. Ristow and T. Rühl, "Fourier finite-difference migration," *Geophysics*, vol. 59, no. 12, pp. 1882–1893, Dec. 1994.

[20] R. Wu, "Wide-angle elastic wave one-way propagation in heterogeneous media and an elastic wave complex-screen method," *J. Geophys. Res., Solid Earth*, vol. 99, no. B1, pp. 751–766, Jan. 1994.

[21] M. N. Guddati and A. H. Heidari, "Migration with arbitrarily wide-angle wave equations," *Geophysics*, vol. 70, no. 3, pp. S61–S70, May 2005.

[22] J.-H. Zhang, W.-M. Wang, S.-Q. Wang, and Z.-X. Yao, "Optimized Chebyshev Fourier migration: A wide-angle dual-domain method for media with strong velocity contrasts," *Geophysics*, vol. 75, no. 2, pp. S23–S34, Mar. 2010.

[23] M. Davydenko, "Full wavefield migration: Seismic imaging using multiple scattering effects," Ph.D. thesis, Delft University of Technol., Delft, The Netherlands, 2016, doi: 10.4233/uuid:1cda75d5-8998-49fe-997e-b38c9b7f8b8b.

[24] J. L. T. Grimbergen, F. J. Dessing, and K. Wapenaar, "Modal expansion of one-way operators in laterally varying media," *Geophysics*, vol. 63, no. 3, pp. 995–1005, May 1998.

[25] H. I. Hammad and D. J. Verschuur, "Joint migration inversion for laterally varying media," in *Proc. 78th EAGE Conf. Exhib.*, 2016, pp. 1–5.

[26] A. Li and X. Liu, "An optimised one-way wave migration method for complex media with arbitrarily varying velocity based on eigen-decomposition," *J. Geophysics Eng.*, vol. 18, no. 5, pp. 776–787, Nov. 2021.

[27] R. H. Stolt, "Migration by Fourier transform," *Geophysics*, vol. 43, no. 1, pp. 23–48, Feb. 1978.

[28] J. W. Thorbecke, K. Wapenaar, and G. Swinnen, "Design of one-way wavefield extrapolation operators, using smooth functions in WLSQ optimization," *Geophysics*, vol. 69, no. 4, pp. 1037–1045, Jul. 2004.

[29] J. C. Strikwerda, *Finite Difference Schemes and Partial Differential Equations*. Philadelphia, PA, USA: SIAM, 2004.

[30] F. Aminzadeh, N. Burkhard, L. Nicoletis, F. Rocca, and K. Wyatt, "SEG/EAEG 3-D modeling project: 2nd update," *Lead. Edge*, vol. 13, no. 9, pp. 949–952, Sep. 1994.

Anyu Li received the B.Sc. and M.Sc. degrees from the Department of Geophysics and Information Technology, China University of Geosciences, Beijing, China, in 2014 and 2020, respectively. From 2020 to 2024, he finished his Ph.D. degree at China University of Geosciences.

In 2022, he studied as a visiting student at Delft University of Technology, Delft, The Netherlands. His main research fields are wave propagation, seismic data processing, wave-equation depth migration, and imaging.

Dirk J. (Eric) Verschuur received the M.Sc. and Ph.D. (Hons.) degrees in applied physics from Delft University of Technology, Delft, The Netherlands, in 1986 and 1991, respectively.

From 1992 to 1997, he was a Senior Research Fellowship at the Royal Dutch Academy of Art and Sciences, Amsterdam, The Netherlands. In 1997, he became an Assistant Professor at Delft University of Technology, where he has been an Associate Professor since 1998. He is currently the Director of the Delphi Research Consortium. His main interests are seismic modeling, data processing, and imaging techniques.

Dr. Verschuur received the Society of Exploration Geophysicists's J. Clarence Karcher Award in 1997. He was awarded the Virgil Kauffman Gold Medal from SEG in 2006.

Xuewei Liu received the B.Sc. and M.Sc. degrees from Jilin University, Changchun, China, in 1982 and 1985, respectively, and the Ph.D. degree from the Department of Automation at Tsinghua University, Beijing, China, in 1991.

He received funding from the Royal Society to work at Durham University, Durham, U.K. from 1997 to 1998. Currently, he is a Professor at the China University of Geosciences, Beijing. His research interests are seismic signal processing, wave theory, imaging techniques under complex seismic geological conditions, and seismic identification of natural gas hydrates.

Siamak Abolhassani received the master's degree in exploration seismology from the Institute of Geophysics, University of Tehran, Tehran, Iran, in 2016, with a thesis focused on full waveform inversion.

He is currently a Ph.D. Researcher at Delft University of Technology, Delft, The Netherlands, where he collaborates with Dr. Dirk J. (Eric) Verschuur at the Delphi Research Consortium, developing high-resolution reflection waveform tomography tools. His main research interest lies at the intersection of wave theory and inverse theory.